# Quantification of the water age and submarine groundwater discharge in a typical semi-enclosed bay: Using stable oxygen ($^{18}$O) and radioactive radium ($^{228}$Ra) isotopes

Qianqian Wang [1, 2#]; Xiaolang Zhang [1, 2, 4#]; Xuejing Wang [1, 2*]; Kai Xiao [1, 2]; Yan Zhang [3]; Linlin Wang[1, 2]; Xingxing Kuang [1, 2]; Hailong Li [1, 2, 3]

[1] *State Environmental Protection Key Laboratory of Integrated Surface Water-Groundwater Pollution Control, School of Environmental Science and Engineering, Southern University of Science and Technology, Shenzhen, Guangdong 518055, China*

[2] *School of Environmental Science and Engineering, Guangdong Provincial Key Laboratory of Soil and Groundwater Pollution Control, Southern University of Science and Technology, Shenzhen, Guangdong 518055, China*

[3] *MOE Key Laboratory of Groundwater Circulation & Environment Evolution and School of Water Resources and Environment, China University of Geosciences (Beijing), Beijing 100083, China*

[4] *Department of Earth Sciences, The University of Hong Kong, Hong Kong, China*

[#]These authors contributed equally to this work and should be considered co-first authors.

[*]Corresponding author: Xuejing Wang (wangxj3@sustech.edu.cn)

## Abstract

Nutrient inputs through submarine groundwater discharge (SGD) play a significant role in sustaining primary productivity and nutrient cycling in coastal areas. Currently, various geochemical isotopes are used to trace the SGD processes. However, mass balance models of stable water isotopes ($^{2}$H and $^{18}$O) are seldom used in SGD estimating. In this study, mass balance models of $^{18}$O and radium isotopes were used to estimate the water age and SGD in Laizhou Bay, China based on the isotope data sampled in August 2017. The water age ranged from 23.5 to 50.0 days with an average of 32.1 ± 16.3 days. The SGD flux ranged from $1.29 \times 10^{8}$ m$^{3}$ d$^{-1}$ to $2.84 \times 10^{8}$ m$^{3}$ d$^{-1}$ with an average of $(2.07 \pm 1.04) \times 10^{8}$ m$^{3}$ d$^{-1}$. The sensitivity analysis revealed that estimated results of the water age and SGD are very sensitive to the $^{18}$O value in evaporation, as well as $^{18}$O and $^{228}$Ra values in groundwater end-members. Based on the isotope method, the proportion of the Yellow River discharging into Laizhou Bay was estimated to be less than 27% of the total discharge. Furthermore, combining water and salt mass balance models, the submarine fresh groundwater discharge (SFGD) flux ranged from $0.54 \times 10^{7}$ m$^{3}$ d$^{-1}$ to $1.31 \times 10^{7}$ m$^{3}$ d$^{-1}$ with an average of $(0.93 \pm 0.46) \times 10^{7}$ m$^{3}$ d$^{-1}$. This study reveals that stable and radium isotopes can be effectively combined to estimate the water age and SGD, which may be applied to coastal areas elsewhere.

**Keywords**: Coastal groundwater; Hydrogen and oxygen isotopes; Radium isotopes; Submarine fresh groundwater discharge; Nutrient loading; Laizhou Bay

## 1. Introduction

Submarine groundwater discharge (SGD) has been recognized as an important component of the global water cycle, and it is a significant pathway for delivering terrestrial substances to the ocean (Moore, 1996; Burnett et al., 2003; Michael et al., 2016; Santos et al., 2021). The studies on SGD are increasingly carried out in different regions and countries around the world (Cho & Kim, 2016; Moosdorf & Oehler, 2017; Zhang et al., 2020). SGD typically comprises submarine fresh groundwater discharge (SFGD) and recirculated saline groundwater discharge (RSGD). Increasing studies have revealed that various environmental problems such as harmful algal blooms in coastal waters are closely related to SGD-associated nutrients (Lee & Kim, 2007; Luo & Jiao, 2016; Chen et al., 2020). Therefore, evaluating the magnitude of SGD and associated nutrient fluxes is vital for protecting and managing marine ecological environments in the coastal area.

The water age is essential to understanding the hydrodynamic processes, and it is also a key parameter in the calculation process of SGD. Radium isotopes have been widely used to estimate water age and SGD at different spatial and temporal scales (Moore et al., 2006; Rodellas et al., 2017; Wang et al., 2019). The radium-derived water ages represent the time it took for radium isotopes to enter into the system via their sources (Zhang et al., 2020). Moore (2000) built a simple but sagacious model based on radium isotopes to derive the water age of continental shelf. Moore et al. (2006) proposed another mass model of radium isotope by considering all sources and sinks to estimate the water age. The two models have been widely used to estimate the water age in coastal regions worldwide (Xu et al., 2013; Sadat-Noori et al., 2015; Peternann et al., 2018). However, different models have site-specific assumptions. For example, the model from Moore (2000) is not applicable to estuaries and salt marshes where radium additions from sediments and groundwater are continuous. The model of Moore et al. (2006) may be misused by quite a few successive investigators without checking all the site-specific conditions in their case study sites (Zhang et al., 2020). Therefore, evaluating the water age is still challenging because all the site-specific conditions need to consider in the coastal area.

Radium (Ra) isotopes are significantly enriched in both brackish groundwater and nearshore pore water, making Ra an ideal tool for tracing SGD processes in the coastal area (Garcia-Orellana et al., 2014; Tamborski et al., 2017; Nakajima et al., 2021). Stable hydrogen ( $^{2}$H) and oxygen ( $^{18}$O) isotopes are useful conservative tracers for the mixing processes at the groundwater-seawater interface because they clearly distinguish between terrestrial groundwater and seawater (Povinec et al., 2008). They have been increasingly used to construct an end-member mixing model to distinguish the source of groundwater discharge (Povinec et al., 2008; Chaillou et al., 2018; Wang et al., 2021). For example, Petermann et al. (2018) built four end-member mixing model of stable and

radioactivity isotopes to estimate fractions of seawater. Debnath et al. (2019) used two end-member mixing model of $^{18}O$ to distinguish groundwater from SGD. However, there are few studies to estimate SGD flux using mass balance models of stable isotopes in the coastal area.

The current study was conducted to estimate the water age and SGD by combining stable water and radium isotope mass balance models. This study was conducted in Laizhou Bay (China), a vertically well mixed semi-enclosed embayment. The SFGD flux was also estimated by combining water and salt mass balance models. Nutrient fluxes from SGD were estimated based on the estimated SGD flux,

## 1. Materials and methods

### (a) Study area

Laizhou Bay (37.05°-37.80°N, 118.90°-120.35°E), one of three major bays of Bohai Sea, is located in the north of the Shandong peninsula in China (Fig. 1). Laizhou Bay has an overall surface area of ~6000 $km^2$, and it is a typical semi-enclosed bay with an average water depth of 8 m and a maximum water depth of ~15 m at the east mouth of the bay (Wang et al., 2020a). The natural coastline of Laizhou Bay, with a length of ~320 km, extends from the Qimu Cape to the Yellow River estuary. Seawater in the bay is vertically well mixed and can be treated as a single layer (Wang et al., 2015b; Wang et al., 2020a). The Yellow River, as the fifth largest river in the world, is the largest one discharging into Laizhou Bay. It carries large amounts of sediments, forming a cluster of sand bars at the river mouth (Xu et al., 2013; Wang et al., 2019). The mouth of the Yellow River is located between Bohai Bay and Laizhou Bay.

The tides in the region are composed of a mixture of semidiurnal and diurnal components, which are also affected by the natural development of the Yellow River delta and the coastline changes resulting from large-scale anthropogenic land reclamation and fishing farms (Pelling et al., 2013).

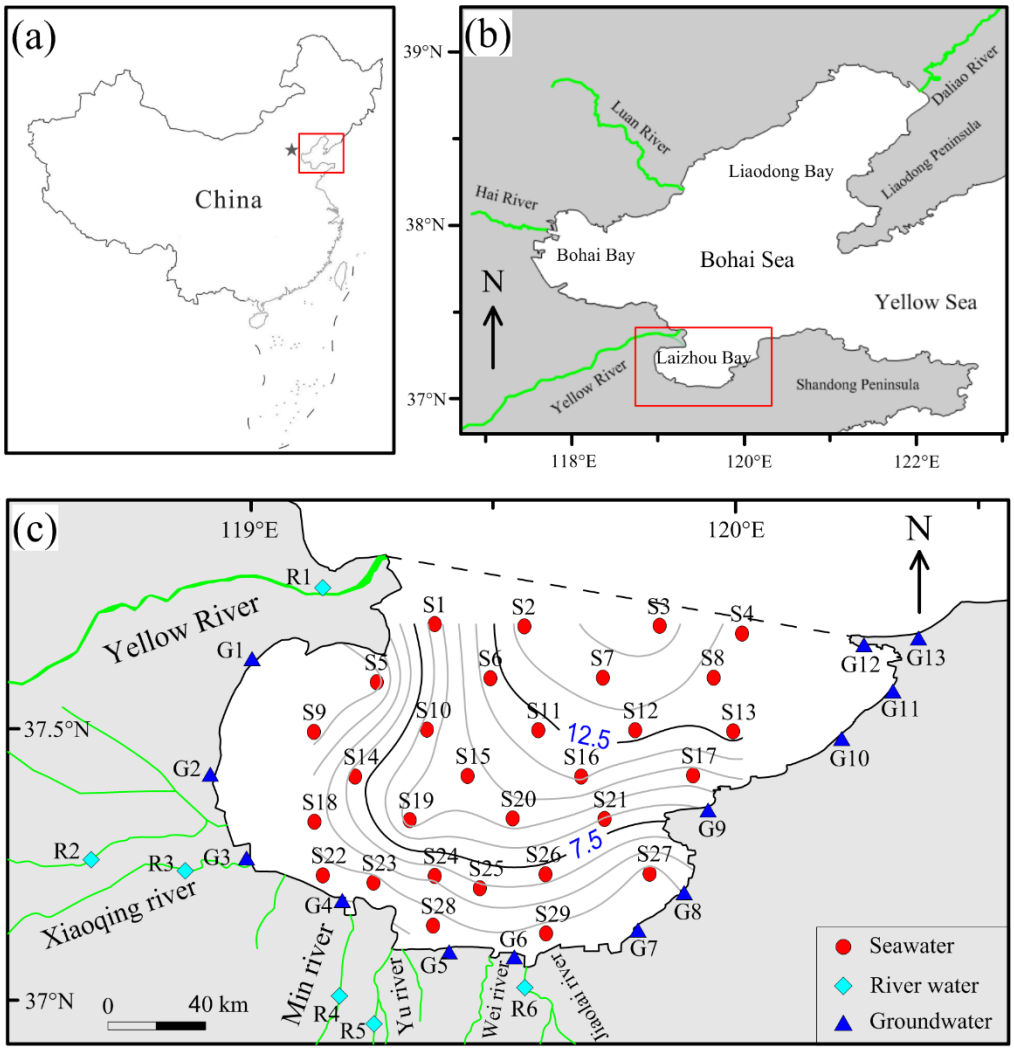


**Fig. 1.** Map of study area: (a) the relative locations of Bohai Sea to Mainland China; (b) the specific location of Laizhou Bay in Bohai Sea; (c) the spatial distribution of sampling locations. The lines with marked numbers 7.5 and 12.5 are water depth (m) contours with respect to mean sea level. The red circles, blue triangle and green diamond indicate the sampling locations of seawater, groundwater and river water, respectively.

## 1. Sampling and analytical methods

The sampling campaign was conducted in August 2017. The sampling stations are shown in Fig.1. Samples of Ra isotopes were collected from the methods proposed by Moore & Reid (1973). Seawater samples (60 L) for Ra isotopes were collected at depths of 2 m below the water surface. River water samples

(30 L) for Ra isotopes were collected at a depth of 1 m below the water surface. Groundwater samples (2-10 L) for Ra isotopes were taken using a push-point sampler at the depths ranging from 0.5 m to 1.5 m in the intertidal zone. Water samples for Ra isotopes were filtered through ~25 g of manganese-coated acrylic fiber (Mn-fibers) at a flow rate of less than 1 L $min^{-1}$ to absorb dissolved Ra (Moore & Reid, 1973). These Mn-fibers were then washed thoroughly using distilled water to remove any particles and salts.

Water samples for stable isotopes ( $^{18}O$ and $^{2}H$) at each station were filtered through a 0.45- m membrane filter. Samples for stable isotopes were collected in 15-mL polyethylene bottles with no headspace. Nutrient samples were also filtered through a 0.45- m membrane filter. All samples were stored at 4-6°C until laboratory measurements. In addition, water samples for salinity and temperature at each station were measured in situ using a handheld HI9828 multi-parameter water quality meter (HANNA).

The activity of $^{228}Ra$ was measured by Radium Delayed Coincidence Counter (RaDeCC) using the method proposed by Moore & Arnold (1996). The activity of $^{228}Ra$ was determined by measuring $^{228}Th$ ingrown from $^{228}Ra$ and calculating the initial $^{228}Ra$ (Moore et al., 2008; Charette et al., 2008). The uncertainty of $^{228}Ra$ in the lab system was ~7%. The values of stable water isotopes were determined by off-axis integrated cavity output spectroscopy (OA-ICOS) (LGR, DLC-100). The $^{18}O$ and $^{2}H$ measurements were reported relative to the Vienna Standard Mean Ocean Water (VSMOW). The $^{18}O$ and $^{2}H$ values were reported in the conventional delta ( ) notation and in per mil (‰). The analytical precisions were 0.1‰ for $^{18}O$ and 0.3‰ for $^{2}H$.

1. **Theoretical models**

2.3.1 Stable isotope mass balance

Under steady-state conditions, water inputs in the system were mainly from precipitation, river and submarine fresh groundwater discharge. Water outputs in the system included mixing with open sea water and evaporation. Stable isotope mass balance model was based on water mass balance model (Petermann et al., 2018). The $^{2}H$ was not used here because it is relatively high sensitivity in temperature and humidity (Stalker et al., 2009) and it was well correlated with $^{18}O$ ($R^2$=0.99, $n$=54). Therefore, $^{18}O$ mass balance model can be expressed as equation (1).

(1)

where is SGD flux; is river discharge; and are input and output of water from precipitation and evaporation; , and are $^{18}O$ values in SGD, river water and open sea water, respectively. and are $^{18}O$ values in precipitation and evaporation, respectively. is the inventory of $^{18}O$ in the bay; is the total water volume in the bay; is water age of the bay. Here, values are defined as isotopic ratios reflecting deviation in per mil from Vienna-SMOW (Standard Mean Ocean Water) (Gibson et al., 2016).

In equation (1), , , , and can be directly measured. Direct observation of the isotopic composition of evaporating water, , is not technically feasible, but can be estimated using the linear resistance model proposed by Craig & Gordon (1965):

(2)

where is the relative humidity normalized to surface water temperature (decimal fraction), is the total fractionation factor (; Krabbenhoft, 1990; Stets et al., 2010); is the diffusion controlled or the kinetic fractionation factor (; Krabbenhoft, 1990); is an empirical constant relating to the kinetic fractionation factor and relative humidity and it was 14.3 (Gibson and Reid, 2010); is the equilibrium isotopic fractionation factor at the temperature of the air-water interface, which is related to temperature () as (Stets et al., 2010); is the isotopic composition of atmospheric moisture, which can be estimated by (Stets et al., 2010).

2.3.2 Radium mass balance

Ra sources in the system were mainly from SGD, rivers, diffusion from bottom sediments and atmospheric dust. River inputs include the dissolved portion and desorbed portion from suspended particulate matter (SPM). In this study, we only considered SPM in the Yellow River, which accounted for >90% of total SPM flux in Laizhou bay. Ra sinks in the system generally included radioactive decay and mixing loss with open sea water. Especially, in the approach proposed by Peterson et al. (2008), the average of two low-activity values of Ra in the bay water is used as an indicator of the background activity. These background activities can be regarded as containing the contributions from bottom sediments and atmospheric dust. Here, $^{228}$Ra was selected to build a mass balance model because it has a long-life and low uncertainty; the decay loss of $^{228}$Ra can be neglected. Therefore, $^{228}$Ra mass balance model in the system can be expressed as equation (2).

(5)

Where , and are $^{228}$Ra activity in SGD, river water and open sea water, respectively; is the inventory of $^{228}$Ra in the bay; is the decay constant of $^{228}$Ra.

2.3.3 Calculations of the water age and SGD

All the parameters in equations (1) and (3) can be derived or estimated from the data collected and the literature. The only exceptions are the water age and SGD flux. We thus combined equations (1) and (3) to solve the unknown parameters (i.e., the water age and SGD flux).

2.3.4 Calculation of SFGD

From the method proposed by Wang et al. (2015b), SFGD flux can be estimated by combining water mass balance and salt mass balance:

(6)

where is the inventory of salt in the bay; is the salinity in open sea water.

1. **Results**

(a) Salinity, $^{228}$Ra and stable isotope distributions

Data for salinity, $^{228}$Ra and stable ( $^{2}$H and $^{18}$O) isotopes in seawater are shown in Supporting Table S1. During the sampling period, the salinity of seawater ranged from 25.21 to 31.92 with an average value of 30.10. The salinity generally increased from the nearshore areas to the mouth of the bay (Fig. 2a). The salinity was distinctly higher in the east than that in the west (Fig. 2a), which may be related to the freshwater from the Yellow River.

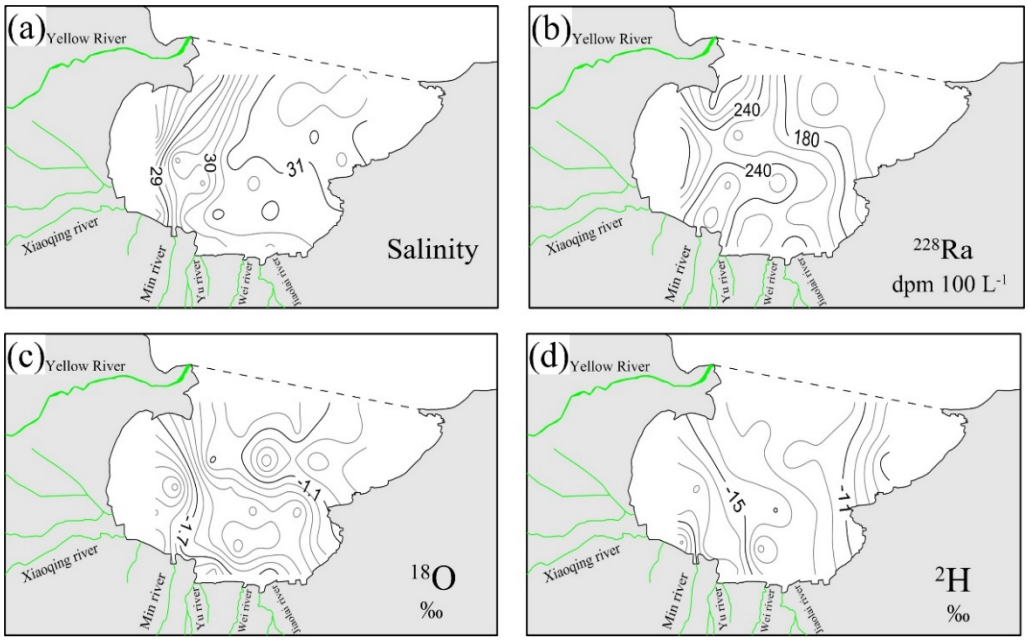


**Fig. 2.** Spatial distributions of salinity, $^{228}$Ra and stable isotopes ( $^{2}$H and $^{18}$O) in seawater

Activities of $^{228}$Ra in seawater ranged from 120.54 to 305.57 dpm 100 $L^{-1}$ with an average value of 204.55 dpm 100 $L^{-1}$. Activities of $^{228}$Ra generally decreased from the nearshore areas to the mouth of the bay (Fig. 2b). The elevated activities of $^{228}$Ra were located near the southern coast and the mouth of the Yellow River.

The values of $^{2}$H in seawater ranged from -22.16 to -6.44 ‰ with an average value of -13.49 ‰. The value of $^{18}$O in seawater ranged from -2.25 to -0.71 ‰ with an average value of -1.36 ‰. The $^{2}$H and $^{18}$O had the similar distributions with salinity.

Data for salinity, $^{228}$Ra and stable ( $^{2}$H and $^{18}$O) isotopes in groundwater and river water are shown in Supporting Table S2 and S3. Figs 3a-3c show the relationships between $^{228}$Ra and stable isotopes versus salinity in all samples.

Activities of $^{228}$Ra in groundwater were higher than those in seawater and river water, suggesting that the groundwater discharge may be a major source of $^{228}$Ra in the bay. On the other hand, values of $^{2}$H and $^{18}$O in river water were significantly lower than those in groundwater and seawater. The high depletion of $^{2}$H and $^{18}$O in river water suggests significantly evaporation rates in river water. Values of $^{2}$H and $^{18}$O in all samples ( $^{2}$H=6.9593 × $^{18}$O-4.3432, $R^2$=0.9668) deviated from the global meteoric water line (GMWL) and the local meteoric water line (LMWL), also suggesting the influence of evaporation.

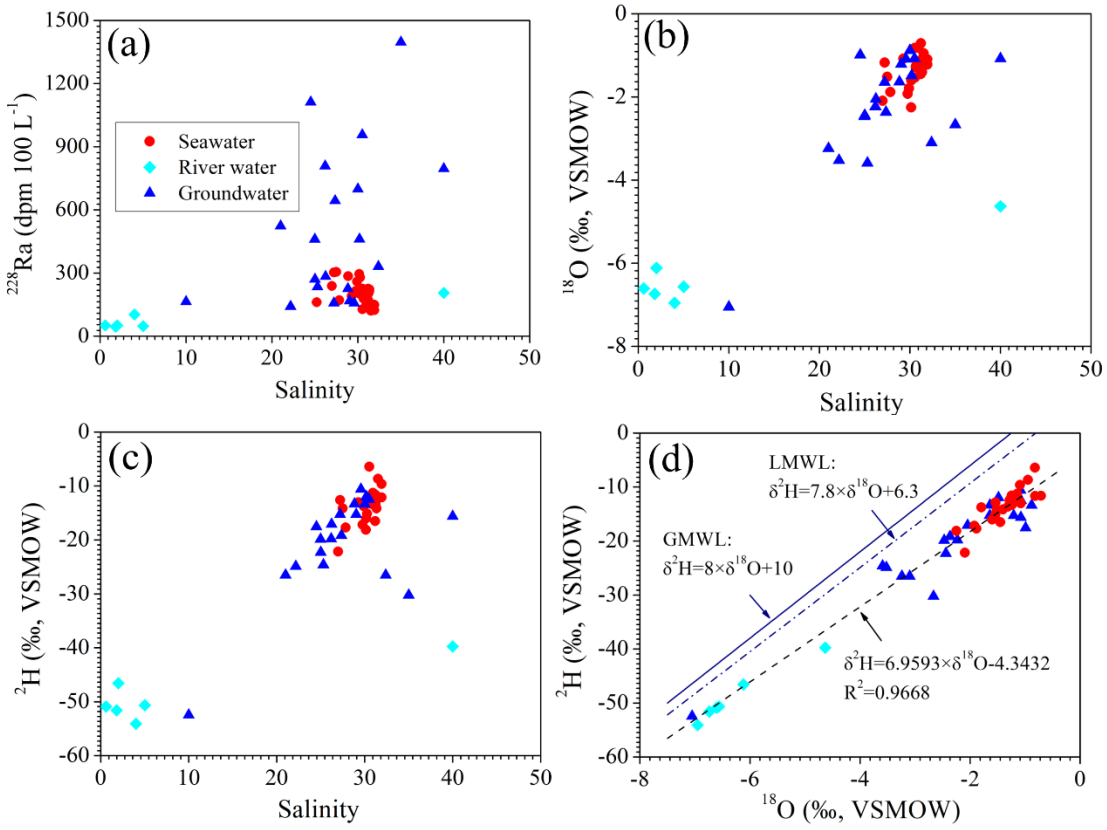


**Fig. 3.** Salinity, $^{228}$Ra and stable isotopes in all samples (a) $^{228}$Ra versus salinity; (b) $^{18}$O versus salinity; (c) $^{2}$H versus salinity; (d) $^{2}$H versus $^{18}$O. The global meteoric water line (GMWL) was from Craig (1961) and the local meteoric water line (LMWL) was from Han et al. (2011).

### 3.2 Fluxes of $^{228}$Ra and $^{18}$O from rivers

The flux of $^{228}$Ra from the river generally consists of the dissolved portion and desorption portion from suspended sediments. The Yellow River delivers large amounts of water and suspended sediments to the Bohai Sea (Yang et al., 2019). The discharge of the Yellow River in August 2017 was 8.48 × $10^8$ $m^3$ $d^{-1}$. The

flux of SPM from the Yellow River in August 2017 was $2.07 \times 10^7$ kg $d^{-1}$. These data of the Yellow River was obtained from the Yellow River Water Resources Bulletin published by the Yellow River conservancy commission of the Ministry of Water Resources of China in 2017. Combining the desorption rate of 2000 dpm $kg^{-1}$ for $^{228}Ra$ from SPM (Moore et al., 2008; Wang et al., 2019), the total flux of $^{228}Ra$ from the Yellow River was estimated to be $(5.58 \pm 0.62) \times 10^{10}$ dpm $d^{-1}$. The discharge of rivers other than the Yellow River during the corresponding sampling period was $2.70 \times 10^6$ $m^3$ $d^{-1}$. The flux of $^{228}Ra$ from rivers other than the Yellow River was estimated to be $(2.14 \pm 0.62) \times 10^9$ dpm $d^{-1}$.

The flux of $^{18}O$ from the Yellow River was estimated to be $-1.87 \times 10^8$ ‰. The flux of $^{18}O$ from rivers other than the Yellow River during the sampling period was estimated to be $-1.70 \times 10^7$ ‰.

3.3 Inventories of $^{228}Ra$ and $^{18}O$

The evaluation of $^{228}Ra$ (or $^{18}O$) inventory is key to estimate SGD when using the mass balance model because it directly significantly affects the mixing loss with open sea water (Savatier & Rocha, 2021). In this study, the study area was divided into 78 sections (triangular elements) so that each of the sampling stations is a vertex of a triangular element (Supporting Fig. S1). The inventory of $^{228}Ra$ (or $^{18}O$) in the total study area was calculated as the sum of $^{228}Ra$ (or $^{18}O$) inventory in each triangular element. The $^{228}Ra$ (or $^{18}O$) inventory in each triangular element was calculated as the product of the volume of the seawater and the average activities of $^{228}Ra$ (or $^{18}O$) at three vertices of the triangular element. The volume of the seawater in each triangular element was calculated as the product of the area of the corresponding triangular element and the averaged seawater depths at the three vertices of the element.

The total seawater area and volume of Laizhou Bay were estimated to be $6.87 \times 10^9$ $m^2$ and $4.62 \times 10^{10}$ $m^3$, respectively. Inventories of $^{228}Ra$ and $^{18}O$ were estimated to be $(8.87 \pm 0.62) \times 10^{13}$ dpm and $-5.72 \times 10^{10}$ ‰, respectively.

3.4 Values of $^{18}O$ in the evaporation and precipitation

Samples of $^{18}O$ in seawater deviated significantly from the LMWL as a consequence of isotopic enrichment of seawater due to evaporate (Fig. 3d). Here, the value of $^{18}O$ in the evaporation was estimated from equation (2). Parameter values in equation (2) are shown in Table 1. The value of $^{18}O$ in the evaporation in Laizhou Bay was then estimated to be -23.47 ‰. Gibson et al. (2016) estimated the value of $^{18}O$ in the evaporation ranging from -20.00 ‰ to -54.15 ‰ in coastal and continental areas. Our estimated result was within the ranges of their results.

The value of $^{18}O$ in the precipitation was -7.0 ‰ from the direct measurement based on the rainfall monitored at Yantai stations in Shandong province, China (Han et al., 2011).

3.5 Values of $^{228}Ra$ and $^{18}O$ in the open sea water

The activity of $^{228}$Ra in the open sea water was determined using the lowest-activity $^{228}$Ra at station S4. Similarly, the value of $^{18}$O in the open sea water is determined using the value of $^{18}$O at station S4. The station S4 was closest to the open sea and farthest from the coastline among all the offshore stations (Fig. 1). Therefore, the activity of $^{228}$Ra in the open sea water was 120.54 dpm 100 $L^{-1}$, and the value of $^{18}$O in the open sea water was -0.95 ‰.

1. **Discussion**

4.1 Water age and SGD estimations

The parameter values in equations (1) and (3) are listed in Table 2. Fig. 4a shows how the water age changes with the proportion of the Yellow River input into Laizhou Bay (). One can see that the water age increases as increases. When = 0, the water age was estimated to be 23.5 ± 11.8 d. Hainbucher et al. (2004) modeled seawater circulation in the Bohai Sea and determined the water age (defined as "turnover time") in different areas of the Bohai Sea. Their results suggest that Laizhou Bay's water age is in the range of 15-40 d. Based on the radium isotope model and the tidal prism method, Wang et al. (2015b) obtained a water age estimation of 36.6 ± 5.3 d of Laizhou Bay. Wang et al. (2020a) estimated the water age of Laizhou Bay ranging from 15 to 50 d using radium quartet mass balance models. From above-mentioned estimated water age of Laizhou Bay, it is reasonable to assume that the water age of Laizhou Bay is less than 50 d. Combining our estimated water age, therefore, we can conclude the water age of Laizhou Bay ranging from 23.5 to 50.0 d with an average of 32.1 ± 16.3 d. Thus, we can obtain the reasonable value of ranging from 0 to 0.27 with an average of 0.14. Namely, the proportion of the Yellow River discharging into Laizhou Bay was less than 27% of the total discharge during the sampling period. The Yellow River mouth is northerly-oriented, which may limit the input of the Yellow River into Laizhou Bay (Xu et al., 2013). Wang et al. (2015b) also reported the value of was less than 0.14 in August 2012 from the radium isotope method.

Fig. 4b shows how the SGD flux changes with the proportion of the Yellow River input into Laizhou Bay (). One can see that the SGD flux decreases as increases. When = 0, the SGD flux was estimated to be (2.84 ± 1.42) × $10^8$ $m^3$ $d^{-1}$. Based on the above estimated ranging from 0 to 0.27, the SGD flux ranged from 2.84 × $10^8$ $m^3$ $d^{-1}$ to 1.29 × $10^8$ $m^3$ $d^{-1}$ with an average of (2.07 ± 1.04) × $10^8$ $m^3$ $d^{-1}$. The estimated SGD flux was an order of magnitude larger than the discharge of the Yellow River during the sampling period.

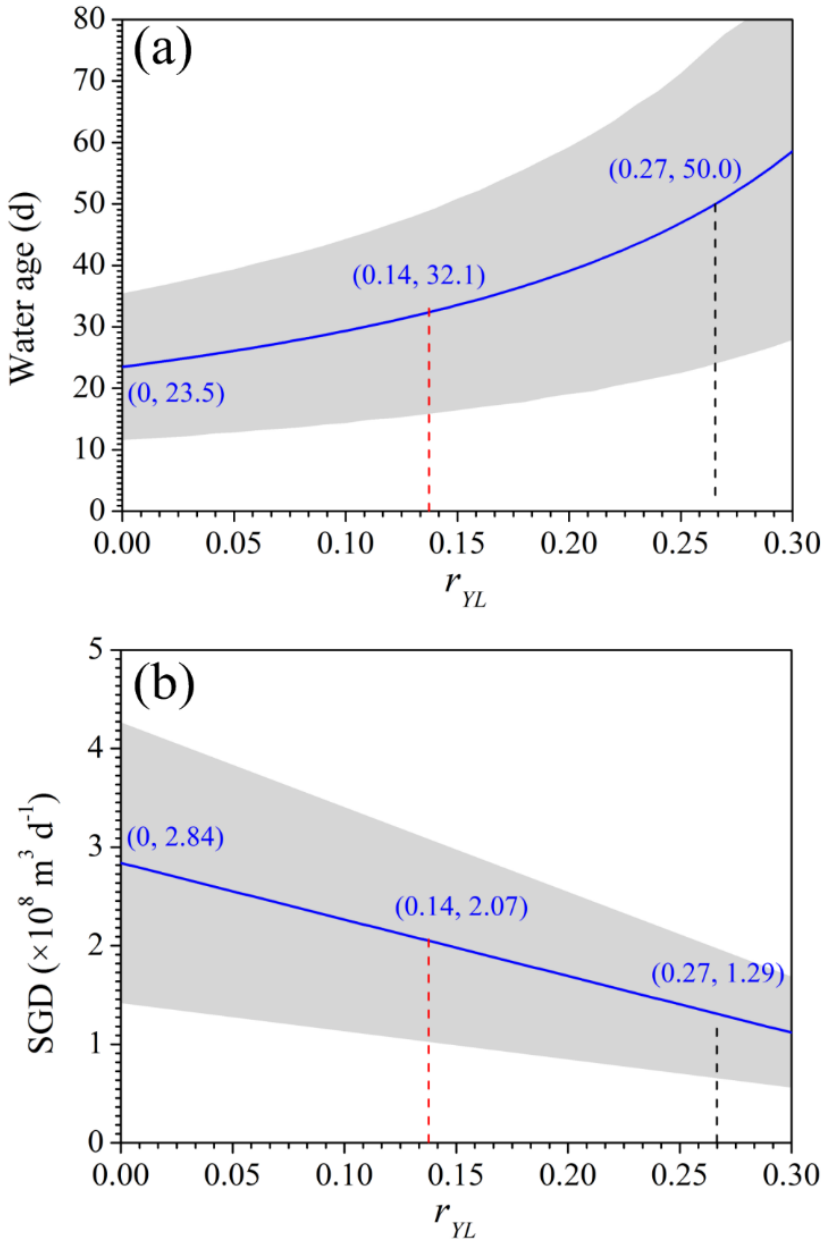


**Fig. 4.** Changes of water age (a) and SGD (b) with the proportion of the Yellow River input into Laizhou Bay. The value of ranged from 0 to 0.27. The red vertical dashed line represents the average value of . The blue bands bounded by the pair of dotted-lines represent the error ranges.

4.2 SFGD estimation

Fig. 5 shows how the SFGD flux changes with the proportion of the Yellow River input into Laizhou Bay (). One can see that the SFGD flux decreases as increases. When = 0, the SGD flux was estimated to be (1.31 ± 0.65) × $10^7$ $m^3$ $d^{-1}$. Based on the above estimated ranging from 0 to 0.27, the SFGD flux ranged from 0.54 × $10^7$ $m^3$ $d^{-1}$ to 1.31 × $10^7$ $m^3$ $d^{-1}$ with an average of (0.93 ± 0.46) × $10^7$ $m^3$ $d^{-1}$. Compared with the estimated SGD, the value of had a significant influence on the estimated SFGD. The estimated SFGD flux was 0.19-0.45 times the discharge of the Yellow River during the sampling period. From Fig. 5, one can also see that the value of was less than 0.46, which suggests that it is reasonable to assume the water age of Laizhou Bay ranging from 0 to 0.27.

In addition, the ratio of SFGD to SGD ranged from 4.3% to 4.6% with an average of 4.5%. On the other hand, RSGD is the main component of SGD. Previous regional investigations also reported that SFGD typically represents less than 10% of the total SGD at several sites worldwide (Beck et al., 2008; Tanuguchi et al., 2008; Santos et al., 2011).

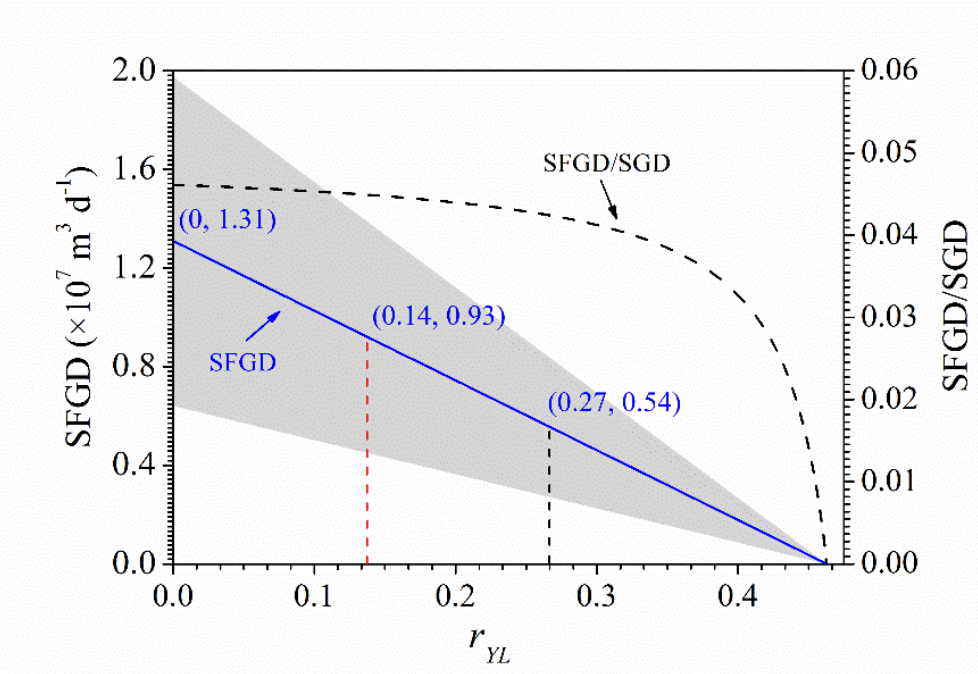


**Fig. 5.** Changes of SFGD and SFGD/SGD with the proportion of the Yellow River input into Laizhou Bay. The ratio of SFGD to SGD is shown on the right-axis. The value of ranged from 0 to 0.27. The red vertical dashed lines represent the average value of . The red vertical dashed line represents the average value of .

4.3. Comparisons with previous studies

Table 3 shows the estimated SGD flux in Laizhou Bay in several previous studies during different periods. Our results, if using the same unit, ranged from 2.2 to 4.7 cm $d^{-1}$. The differences among these reported results mainly may be attributed to different tracers and methods as well as the sampling periods. For example, in general, the relatively high SGD flux estimated by $^{222}Rn$ mass balance is because $^{222}Rn$ traces the total SGD including fresh and brackish groundwater (Luo & Jiao, 2016). Radium isotopes mainly trace the brackish groundwater discharge. On the other hand, previous studies have revealed seasonal variations of SGD (e.g., Moore et al., 2006; Wang et al., 2015a). These variations may be related to precipitation and sea level change (Wang et al., 2015a; Chen et al., 2017). Overall, our results were within the ranges of the results reported by previous studies.

Wang et al. (2019) used radium isotopes to estimate SGD flux in Bohai Bay, China. They estimated that SGD flux of Bohai Bay ranged 2.0 to 4.8 cm $d^{-1}$. Our result was similar to the SGD flux of Bohai Bay, where the hydrological conditions are similar to those of Laizhou Bay. In addition, the coastline length of Laizhou Bay was 320 km (Wang et al., 2020a). When scaled to the coastline length, the SGD flux ranged from $4.0 \times 10^7$ $m^3$ $m^{-1}$ $d^{-1}$ to $8.9 \times 10^7$ $m^3$ $m^{-1}$ $d^{-1}$. Our result was at the same order of magnitude of the global average SGD flux (Kwon et al., 2014). These would provide additional confidence in the result estimated by combining stable water and radium isotope mass balances models.

4.4 Uncertainty and sensitivity analysis

Selecting representative end-members of $^{18}O$ and $^{228}Ra$ in mass balance models is of great importance to estimate the water age and SGD. In this study, we used sensitivity analysis to discuss the impact of different end-members on the estimated results. Since the value of was unknown, both the minimum value =0 and maximum value =0.27 were used in the following discussion.

Sensitivity analysis was performed to examine the contribution of single parameter to the water age and SGD by increasing and decreasing the parameter by 10% without changing the other parameters. In this study, end-members of $^{18}O$ and $^{228}Ra$ in precipitation, evaporation, river and groundwater were selected for the sensitivity analysis. Table 4 and Table 5 show sensitivity analysis of the calculated water age and SGD, respectively. Sensitivity analysis shows that $^{18}O$ in precipitation, evaporation and groundwater end-members, as well as $^{228}Ra$ in groundwater end-member have a large influence on both the water age and SGD. In general, $^{18}O$ in precipitation can be directly measured, while direct observation of $^{18}O$ in evaporation is not technically feasible (Gibson et al., 2016). The value of $^{18}O$ in evaporation can be estimated using the theoretical model. Therefore, determining $^{18}O$ value in the evaporation is crucial for estimating the water age and SGD.

On the other hand, $^{228}Ra$ is continuously produced by the decay of uranium and thorium parents in aquifers. $^{228}Ra$ is generally adsorbed onto the particle surface

in freshwater. When exposed to brackish or saline water, $^{228}$Ra rapidly desorbs from the particle surface (Webster et al., 1995; Gonneea et al., 2008). Due to heterogeneity in sediment composition and salinity distribution, the activity of $^{228}$Ra in coastal groundwater could show several orders of magnitude variability (Michael et al., 2011; Duque et al., 2019). In this study, the highest activity of $^{228}$Ra was an order of magnitude higher than the lowest one. The value of $^{18}$O in groundwater at different depths were mainly affected by evaporation. Therefore, the value of $^{18}$O in groundwater can vary widely at the regional scale. Overall, both determining $^{18}$O value in evaporation and selecting $^{18}$O and $^{228}$Ra in groundwater end-members are crucial for estimating the water age and SGD.

4.5 Nutrient fluxes from SGD

Many studies showed that SGD can transport large fluxes of nutrient from land to ocean (Sadat-Noori et al., 2015; Wang et al., 2020b; Selvam et al., 2021). Given that the estimated SGD flux was an order of magnitude larger than the discharge of the local largest river, the Yellow River, SGD may have the significant influence on delivering nutrients to the ocean. In this study, to obtain a conservative estimate of SGD associated nutrient fluxes, the average SGD flux of $(2.07 \pm 1.04) \times 10^8$ m$^3$ d$^{-1}$ was used to calculate. The nutrient fluxes from SGD were calculated as the product of SGD flux and the difference of nutrient concentrations between groundwater and seawater (Wang et al., 2017).

Average nutrient concentrations of TDN, TDP and Si in groundwater were $2.5 \times 10^{-4}$ mol L$^{-1}$, $1.7 \times 10^{-5}$ mol L$^{-1}$ and $2.5 \times 10^{-4}$ mol L$^{-1}$, respectively. Average nutrient concentrations of TDN, TDP and Si in seawater were $4.6 \times 10^{-5}$ mol L$^{-1}$, $5.4 \times 10^{-5}$ mol L$^{-1}$ and $7.9 \times 10^{-6}$ mol L$^{-1}$, respectively. Thus, nutrient fluxes through SGD can be estimated to be $(4.1 \pm 2.1) \times 10^7$ mol d$^{-1}$ for TDN, $(2.0 \pm 1.0) \times 10^6$ mol d$^{-1}$ for TDP and $(4.0 \pm 2.0) \times 10^7$ mol d$^{-1}$ for Si. In general, nutrient is non-conservative behavior due to complex biogeochemical processes and water-rock interactions in groundwater, such as mineralization, nitrification, denitrification and redox reaction (Zhang et al., 2016). Therefore, nutrient fluxes using this method only serve as a rough estimate of input, not absolute input.

The nutrient fluxes from the Yellow River were estimated by multiplying the nutrient concentrations in the Yellow River and the corresponding river discharge. Average concentrations of TDN, TDP and Si in the Yellow River were $1.7 \times 10^{-4}$ mol L$^{-1}$, $0.5 \times 10^{-6}$ mol L$^{-1}$ and $5.5 \times 10^{-5}$ mol L$^{-1}$. Thus, nutrient fluxes from Yellow River were $4.7 \times 10^6$ mol L$^{-1}$ for TDN, $1.5 \times 10^4$ mol L$^{-1}$ for TDP, and $1.5 \times 10^6$ mol L$^{-1}$ for Si. In this study, nutrient fluxes from SGD were higher than those from the Yellow River. Therefore, SGD is recognized as a significant pathway for delivering solute materials from land into the ocean and it may have important effects on the ecosystem environments.

## 1. Conclusions

This study demonstrated a method for estimating the water age and SGD by

combining stable and radium isotope mass balance models. The method was applied in Laizhou Bay, China. The estimated water age ranged from 23.5 to 50.0 days, and the estimated SGD flux ranged from $1.29 \times 10^8$ $m^3$ $d^{-1}$ to $2.84 \times 10^8$ $m^3$ $d^{-1}$. When using this method, both the $^{18}O$ value in evaporation, and $^{18}O$ and $^{228}Ra$ values in groundwater end-members were crucial for estimating the water age and SGD. The geochemical behaviors of stable water and radium isotopes are typically different in groundwater. For a comprehensive understanding of SGD processes, multiple isotope integrated studies is greatly need. By combining water and salt mass balance models, we also estimated SFGD flux in Laizhou Bay. The estimated SFGD flux ranged from $0.54 \times 10^7$ $m^3$ $d^{-1}$ to $1.31 \times 10^7$ $m^3$ $d^{-1}$. The SFGD flux was 0.19-0.45 times the discharge of the Yellow River during the sampling period. Nutrient fluxes from SGD were shown to be significantly higher than those from the Yellow River, which may have important effects on the ecosystem environments.

In addition, based on the isotope method, we estimated the proportion of the Yellow River input into Laizhou Bay. The estimated proportion ranged from 0 to 27%. The proportion would offer instructional information in the management of water resources and sediments in the Yellow River estuary in the future study.

**Data Availability Statement**

The data used to produce the results of this study are available online (https://zenodo.org/record/4902941#.YLso_7czapo).

**Acknowledgments**

This research was supported by the National Natural Science Foundation of China (NOs: 41890852, 41907162, 42077173) and State Environmental Protection Key Laboratory of Integrated Surface Water-Groundwater Pollution Control. The authors thank our team members including Manhua Luo, Wenli Hu, Meiqing Lu, Wei Liu and Yanlan Li for their assistances in field and lab. The authors declare that they have no known competing financial interests.

**References**

Beck, A.J., Rapaglia, J.P., Cochran, J.K., Bokuniewicz, H.J., & Yang, S., 2008. Submarine groundwater discharge to Great South Bay, NY, estimated using Ra isotopes. Marine Chemistry, 109 (3-4), 279-291.

Burnett, W.C., Bokuniewicz, H., Huettel, M., Moore, W.S., & Taniguchi M., 2003. Groundwater and pore water inputs to the coastal zone. Biogeochemistry, 66 (3), 3-33.

Chaillou, G., Lemay-Borduas, F., Larocque, M., Couturier, M., Biehler, A., & Tommi-Morin, G., 2018. Flow and discharge of groundwater from a snowmelt-affected sandy beach. Journal of Hydrology, 557, 4-15.

Charette, M.A., Moore, W.S., & Burnett, W.C., 2008. Uranium- and Thorium-Series Nuclides as Tracers of Submarine Groundwater Discharge (in U-Th Series

Nuclides in Aquatic Systems), in: Radioactivity in the Environment, Radioactivity in the Environment. Elsevier, pp. 155–191.

Chen, X., Lao, Y., Wang, J., Du, J., Liang, M., & Yang, B., 2017. Submarine groundwater-borne nutrients in a tropical bay (Maowei Sea, China) and their impacts on the oyster aquaculture. Geochemistry Geophysics Geosystems, 19, 932-951.

Chen, X., Cukrov, N., Santos, I.R., Rodellas, V., Cukrov, N., & Du, J. (2020). Karstic submarine groundwater discharge into the Mediterranean: Radon-based nutrient fluxes in an anchialine cave and a basin-wide upscaling. Geochimica et Cosmochimica Acta, 268, 467-484.

Cho, H.-M., & Kim, G. (2016). Determining groundwater Ra end-member values for the estimation of the magnitude of submarine groundwater discharge using Ra isotope tracers. Geophysical Research Letters, 43, 3865-3871.

Craig, H. (1961). Isotopic variations in meteoric waters. Science, 133, 1702-1703.

Craig, H., & Gordon, L.I. (1965). Deuterium and oxygen-18 in the ocean and marine atmosphere. In: Tongiorgi, E. (Ed.), Stable Isotopes in Oceanographic Studies and Paleotemperatures, Spoleto, Italy, pp. 9-130.

Debnath, P., Das, K., Mukherjee, A., Ghosh, N.C., Rao, S., Kumar, S., Krishan, G., & Joshi, G. (2019). Seasonal-to-diurnal scale isotopic signatures of tidally-influenced submarine groundwater discharge to the Bay of Bengal: Control of hydrological cycle on tropical oceans. Journal of Hydrology, 571, 124192.

Duque, C., Knee, K.L., Russoniello, C.J., Sherif, M., Abu Risha, U.A., Sturchio, N.C., & Michael, H.A. (2019). Hydrogeological processes and near shore spatial variability of radium and radon isotopes for the characterization of submarine groundwater discharge. Journal of Hydrology, 579, 697-710.

Garcia-Orellana, J., Cochran, J.K., Bokuniewicz, H., Daniel, J.W.R., Rodellas, V., & Heilbrun, C. (2014). Evaluation of 224Ra as a tracer for submarine groundwater discharge in Long Island Sound (NY). Geochimica et Cosmochimica Acta, 141, 314-330.

Gibson, J.J., & Reid, R. (2010). Stable isotope fingerprint of open-water evaporation losses and effective drainage area fluctuations in a subarctic shield watershed. Journal of Hydrology, 381, 142-150.

Gibson, J.J., Birks, S.J., & Yi, Y. (2016). Stable isotope mass balance of lakes: a contemporary perspective. Quaternary Science Reviews, 131, 316-328.

Gonneea, M.E., Morris, P.J., Dulaiova, H., & Charette, M.A. (2008). New perspectives on radium behavior within a subterranean estuary. Marine Chemistry, 109, 250-267.

Han, D., Kohfahl, C., Song, X., Xiao, G., & Yang, J. (2011). Geochemical and isotopic evidence for palaeo-seawater intrusion into the south coast aquifer of

Laizhou Bay, China. Applied Geochemistry, 26, 863-883.

Hainbucher, D., Hao, W., Pohlmann, T., Sundermann, J., & Feng, S.Z. (2004). Variability of the Bohai Sea circulation based on model calculations. Journal of Marine Systems, 44 (3-4), 153-174.

Krabbenhoft, D.P. (1990). Estimating groundwater exchange with lakes 1: The stable isotope mass balance method. Water Resources Research, 26, 2445-2453.

Kwon, E.Y., Kim, G., Primeau, F., Moore, W.S., Cho, H.M., Devries, T., Sarmiento, J.L., Charette, M.A., & Cho, Y.K. (2014). Global estimate of submarine groundwater discharge based on an observationally constrained radium isotope model. Geophysical Research Letters, 41, 8438–8444.

Lee, Y.W., & Kim, G. (2007). Linking groundwater-borne nutrients and dinoflagellate red-tide outbreaks in the southern sea of Korea using a Ra tracer. Estuarine Coastal and Shelf Science, 71, 309-317.

Luo, X., & Jiao, J.J. (2016). Submarine groundwater discharge and nutrient loadings in Tolo Harhor, Hong Kong using multiple geotracer-based models, and their implications of red tide outbreaks. Water Research, 102, 11-31.

Nakajima, T., Sugimoto, R., Kusunoki, T., Yokoyama, K., & Taniguchi, M. (2021). Nutrient fluxes from rivers, groundwater, and the ocean into the coastal embayment along the Sanriku ria coast, Japan. Limnology and Oceanography, 1-17.

Ma, Q., Li, H., Wang, X., Wang, C., Wan, L., Wang, X., Jiang, X. (2015). Estimation of seawater–groundwater exchange rate: case study in a tidal flat with a largescale seepage face (Laizhou Bay, China). Hydrogeology Journal, 23 (2), 265-275.

Michael, H.A., Charette, M.A., & Harvey, C.F. (2011). Patterns and variability of groundwater flow and radium activity at the coast: A case study from Waquoit Bay, Massachusetts. Marine Chemistry, 127, 100-114.

Michael, H.A., Scott, K.C., Koneshloo, M., Yu, X., Khan, M.R., & Li, K. (2016). Geologic influence on groundwater salinity drives large seawater circulation through the continental shelf. Geophysical Research Letters, 43, 10782-10791.

Moore, W.S., & Reid, D.F. (1973). Extraction of radium from natural waters using manganese impregnated acrylic fibers. Journal of Geophysical Research: Oceans, 78, 8880-8886.

Moore, W.S. (1996). Large groundwater inputs to coastal waters revealed by $^{226}$Ra enrichments. Nature, 380, 612-614.

Moore, W.S., & Arnold, R. (1996). Measurement of 223Ra and 224Ra in coastal waters using a delayed coincidence counter. Journal of Geophysical Research: Oceans, 101, 1321-1329.

Moore, W.S. (2000). Ages of continental shelf waters determined from $^{223}$Ra and $^{224}$Ra. Journal of Geophysical Research, 105, 22117-22122.

Moore, W.S., Blanton, J.O., & Joye, S.B. (2006). Estimates of flushing times, submarine groundwater discharge, and nutrient fluxes to Okatee Estuary, South Carolina. Journal of Geophysical Research, 111, C09006.

Moore, W.S., Sarmiento, J.L., & Key, R.M. (2008). Submarine groundwater discharge revealed by 228Ra distribution in the upper Atlantic Ocean. Nature Geoscience, 1, 309-311.

Moosdorf, N., & Oehler, T. (2017). Societal use of fresh submarine groundwater discharge: An overlooked water resource. Earth-Science Reviews, 171, 338-348.

Pelling, H.E., Uehara, K., & Green, J.A.M. (2013). The impact of rapid coastline changes and sea level rise on the tides in the Bohai Sea, China. Journal of Geophysical Research: Oceans, 118 (7), 3462–3472.

Peterson, R.N., Burnett, W.C., Taniguchi, M., Chen, J., Santos, I.R., & Ishitobi, T. (2008). Radon and radium isotope assessment of submarine groundwater discharge in the Yellow River delta, China. Journal of Geophysical Research, 113 (C9).

Petermann, E., Knoller, K., Rocha, C., Scholten, J., Stollberg, R., Weiß, H., & Schubert, M. (2018). Coupling end-member mixing analysis and isotope mass balancing ($^{222}$Rn) for differentiation of fresh and recirculated submarine groundwater discharge into Knysna Estuary, South Africa. Journal of Geophysical Research: Oceans, 123, 1-19.

Povinec, P.P., Bokuniewicz, H., Burnett, W.C., Cable, J., Charette, M., Comanducci, J.-F., Kontar, E.A., Moore, W.S., Oberdorfer, J.A., Oliveira, J., Peterson, R., Stieglitz, T., & Taniguchi, M. (2008). Isotope tracing of submarine groundwater discharge offshore Ubatuba, Brazil: results of the IAEA–UNESCO SGD project. Journal of Environmental Radioactivity, 99, 1596-1610.

Rodellas, V., Garcia-Orellana, J., Trezzi, G., Masque´, P., Stieglitz, T.C., Bokuniewicz, H., Cochran, J.K., & Berdalet, E. (2017). Using the radium quartet to quantify submarine groundwater discharge and porewater exchange. Geochimica et Cosmochimica Acta, 196, 58-73.

Sadat-Noori, M., Santos, I.S., Sanders, C.J., Sanders, L.M., & Maher, D.T. (2015). Groundwater discharge into an estuary using spatially distributed radon time series and radium isotopes. Journal of Hydrology, 528, 703-719.

Santos, I.R., Lechuga-Deveze, C., Peterson, R.N., & Burnett, W.C. (2011). Tracing submarine hydrothermal inputs into a coastal bay in Baja California using radon. Chemical Geology, 282, 1-10.

Santos, I.R., Chen, X., Lecher, A.L., Sawyer, A.H., Moosdorf, N., Rodellas, V., Tamborski, J., Cho, H-M., Dimova, N., Sugimoto, R., Bonaglia, S., Li, H., Hajati, M.., & Li, L. (2021). Submarine groundwater discharge impacts

on coastal nutrient biogeochemistry. Nature Reviews Earth & Environment. https://doi.org/10.1038/s43017-021-00152-0.

Savatier, M., & Rocha, C. (2021). Rethinking tracer-based (Ra, Rn, salinity) approaches to estimate point-source submarine groundwater discharge (SGD) into coastal systems. Journal of Hydrology, 598, 126247.

Selvam, S., Muthukumar, P., Sajeev, S., Venkatramanan, S., Chung, S.Y., Brindha, K., Suresh Babu, D.S., & Murugan, R. (2021). Quantification of submarine groundwater discharge (SGD) using radon, radium tracers and nutrient inputs in Punnakayal, south coast of India. Geoscience Frontiers, 12, 29-38.

Stalker, J.C., Price, R.M., & Swart, P.K. (2009). Determining spatial and temporal inputs of freshwater, including submarine groundwater discharge, to a subtropical estuary using geochemical tracers, Biscayne Bay. South Florida. Estuaries and Coasts, 32, 694-708.

Stets, E.G., Winter, T.C., Rosenberry, D.O., & Striegl, R.G. (2010). Quantification of surface water and groundwater flows to open- and closed-basin lakes in a headwaters watershed using a descriptive oxygen stable isotope model. Water Resources Research, 46, W03515.

Tamborski, J.J., Cochran, J.K., & Bokuniewicz, H.J. (2017). Submarine groundwater discharge driven nitrogen fluxes to Long Island Sound, NY: Terrestrial vs. marine sources. Geochimica et Cosmochimica Acta, 218, 40-57.

Taniguchi, M., Ishitobi, T., Chen, J., Onodera, S.-I., Miyaoka, K., Burnett, W.C., Peterson, R., Liu, G., & Fukushima, Y. (2008). Submarine groundwater discharge from the Yellow River Delta to the Bohai Sea, China. Journal of Geophysical Research, 113, C06025.

Wang, G., Wang, Z., Zhai, W., Moore, W.S., Li, Q., Yan, X., Qi, D., & Jiang, Y. (2015a). Net subterranean estuarine export fluxes of dissolved inorganic C, N, P, Si, and total alkalinity into the Jiulong River estuary, China. Geochimica et Cosmochimica Acta, 149, 103-114.

Wang, X., Li, H., Jiao, J., Barry, D.A., Li, L., Luo, X., Wang, C., Wan, L., Wang, X., Jiang, X., Ma, Q., & Qu, W. (2015b). Submarine fresh groundwater discharge into Laizhou Bay comparable to the Yellow River flux. Scientific Reports, 5, 8814.

Wang, X., Li, H., Luo, X., Jiao, J., Qu, W., & Wang, C. (2016). Using $^{224}$Ra to estimate eddy diffusivity and submarine groundwater discharge in Laizhou Bay, China. Journal of Radioanalytical and Nuclear Chemistry, 308, 403-411.

Wang, X., Li, H., Yang, J., Zheng, C., Zhang, Y., An, A., Zhang, M., & Xiao, K. (2017). Nutrient inputs through submarine groundwater discharge in an embayment: a radon investigation in Daya Bay, China. Journal of Hydrology, 551, 784-792.

Wang, X., Li, H., Zhang, Y., Zheng, C., & Gao, M. (2020a). Investigation of

submarine groundwater discharge and associated nutrient inputs into Laizhou Bay (China) using radium quartet. Marine Pollution Bulletin, 157, 111359.

Wang, Q., Guo, X., & Takeoka, H. (2008). Seasonal variations of the Yellow River plume in the Bohai Sea: a model study. Journal of Geophysical Research, 113, C08046.

Wang, Q., Li, H., Zhang, Y., Wang, X., Zhang, C., Xiao, K., & Qu, W. (2019). Evaluations of submarine groundwater discharge and associated heavy metal fluxes in Bohai Bay, China. Science of the Total Environment, 695, 133873.

Wang, Q., Li, H., Zhang, Y., Wang, X., Xiao, K., Zhang, X., Huang, Y. & Dan, S.F. (2020b). Submarine groundwater discharge and its implication for nutrient budgets in the western Bohai Bay, China. Journal of Environmental Radioactivity, 212, 106132.

Wang, Q., Wang, X., Xiao, K., Zhang, Y., Luo, M., Zheng, C., & Li, H. (2021). Submarine groundwater discharge and associated nutrient fluxes in the Greater Bay Area, China revealed by radium and stable isotopes. Geoscience Frontiers, 12(5), 101223.

Webster, I.T., Hancock, G.J., & Murray, A.S. (1995). Modelling the effect of salinity on radium desorption from sediments. Geochimica et Cosmochimica Acta, 59, 2469-2476.

Xu, B., Burnett, W.C., Dimova, N., Diao, S., Mi, T., Jiang, X., & Yu, Z. (2013). Hydrodynamics in the Yellow River Estuary via radium isotopes: Ecological perspectives. Continental Shelf Research, 66, 19-28.

Zhang, Y., Li, H., Wang, X., Zheng, C., Wang, C., Xiao, K., Wan, L., Wang, X., Jiang, X., & Guo, H. (2016). Estimation of submarine groundwater discharge and associated nutrient fluxes in eastern Laizhou Bay, China using Rn-222. Journal of Hydrology, 533, 103-113

Zhang, Y., Santos, I.R., Li, H., Wang, Q., Xiao, K., Guo, H., & Wang, X. (2020). Submarine groundwater discharge drives coastal water quality and nutrient budgets at small and large scales. Geochimica et Cosmochimica Acta, 290, 201-215.

Yang, D., Xu, B., Burnett, W., Yu, Z., Jiang, X., Zhang, X., Zhao, S., & Xia, D. (2019). Radium isotopes-suspended sediment relationship in a muddy river. Chemosphere, 214, 250–258.

**Table 1** Definitions of parameters and values used in equation (2) to estimate the isotopic composition of evaporating water

| Parameter | Definition | Valu |
|---|---|---|
| $T$ | the surface water temperature | 22 |
| $h$ | the relative humidity | 0.78 |
| $K$ | an empirical constant relating the kinetic fractionation factor and relative humidity [a] | 14.3 |

| Parameter | Definition | Valu |
|---|---|---|
| $\Delta$ | the kinetic fractionation factor | 3.15 |
| | the total fractionation factor | 12.85 |
| $^{*}$ | the equilibrium isotopic fractionation factor at the temperature of the air-water interface | 0.99 |
| $_{A}$ | the isotopic composition of atmospheric moisture | -5.45 |
| $_{E}$ | the isotopic composition of evaporating water | -24.4 |

[a] referring to data from Stets et al. (2010).

**Table 2** Parameters and values used in $^{228}$Ra and $^{18}$O mass balance models.

| Parameter | Value | Definition |
|---|---|---|
| $V_{bay}$ | $4.62\times10^{10}$ | Water volume in the bay ($m^3$) |
| $P_T$ | $5.72\times10^{7}$[a] | Precipitation ($m^3$ $d^{-1}$) |
| $E_T$ | $2.27\times10^{7}$[a] | Evaporation ($m^3$ $d^{-1}$) |
| $I_{Ra}$ | $8.87\times10^{13}$ | Inventory of $^{228}$Ra in the bay (dpm) |
| $I_O$ | $-5.72\times10^{10}$ | Inventory of $^{18}$O in the bay (‰) |
| $Q_{YL}$ | $2.83\times10^{7}$ | Discharge of the Yellow River ($m^3$ $d^{-1}$) |
| $Q_r$ | $2.70\times10^{6}$ | Total discharge of other rivers ($m^3$ $d^{-1}$) |
| $M_{sus}$ | $2.38\times10^{7}$ | Flux of the SPM from the Yellow River (kg $d^{-1}$) |
| $_{des}$ | 2000 | $^{228}$Ra desorption rate (dpm $kg^{-1}$) |
| $_{228}$ | $3.27\times10^{-4}$ | Decay coefficient of $^{228}$Ra ($d^{-1}$) |
| $_{P}$ | -8.0 | Value of $^{18}$O in precipitation (‰) |
| $_{T}$ | -24.4 | Value of $^{18}$O in evaporation (‰) |
| $_{O}$ | -0.95 | Value of $^{18}$O in open sea water (‰) |
| $_{YL}$ | -6.61 | Value of $^{18}$O in the Yellow River (‰) |
| $_{r}$ | -6.30 | Average value of $^{18}$O in other rivers (‰) |
| $_{SGD}$ | -2.29 | Value of $^{18}$O in groundwater (‰) |
| $^{228}Ra_O$ | 120.54 | Activity of $^{228}$Ra in open sea water (dpm 100 $L^{-1}$) |
| $^{228}Ra_{YL}$ | 50.92 | Activity of $^{228}$Ra in the Yellow River (dpm 100 $L^{-1}$) |
| $^{228}Ra_r$ | 79.28 | Average activity of $^{228}$Ra in other rivers (dpm 100 $L^{-1}$) |
| $^{228}Ra_{SGD}$ | 499.79 | Value of $^{18}$O in groundwater (dpm 100 $L^{-1}$) |

[a] The precipitation and evaporation can be calculated as the sum of the total area of study region and average daily precipitation and evaporation occurred during August 2017.

**Table 3** Comparison of SGD with previous studies in Laizhou Bay.

| Laizhou Bay, China | Method | Sampling period |
|---|---|---|
| The Yellow River delta | Radium and radon isotopes<br>Seepage meters | May in 2005, September in 2004 and 2 |
| A tidal flat of Laizhou Bay (Haimiao) | Darcy's law | September in 2014 |

| Laizhou Bay, China | Method | Sampling period |
|---|---|---|
| The eastern Laizhou Bay | $^{222}$Rn | September in 2014 |
| The entire Laizhou Bay | $^{223,\ 226}$Ra | August in 2012 |
| | $^{224}$Ra | August in 2012 |
| | $^{223,\ 224,\ 226,\ 228}$Ra | July-August in 2012 (wet) |
| | | March-April in 2014 (dry) |
| | **$O^{18}$ and $^{228}$Ra** | **August in 2017** |

**Table 4** Sensitivity analysis of the water age. For this analysis, the value of each list below was increased (+) and decreased (-) by 10%, while the other parameters remained unchanged.

| Term (end-member) | % change in the water age with a: | |
|---|---|---|
| | % increase in term value | % decrease in term value |
| $_{YL}$ | +16 | |
| $_{r}$ | +5 | |
| $_{p}$ | **+549** | **-55** |
| $_{T}$ | **-60** | **+308** |
| $_{SGD}$ | **+77** | **-81** |
| $^{228}Ra_{YL}$ | | |
| $^{228}Ra_{r}$ | | |
| $^{228}Ra_{SGD}$ | **-73** | **+86** |
| $_{r}$ | +2 | |
| $_{p}$ | **+133** | **-36** |
| $_{T}$ | **-41** | **+224** |
| $_{SGD}$ | **+81** | **-81** |
| $^{228}Ra_{r}$ | | |
| $^{228}Ra_{SGD}$ | **-74** | **+90** |

**Table 5** Sensitivity analysis of the SGD. For this analysis, the value of each list below was increased (+) and decreased (-) by 10%, while the other parameters remained unchanged.

| Term (end-member) | % change in SGD flux with a: | |
|---|---|---|
| | % increase in term value | % decrease in term value |

| Term (end-member) | % change in SGD flux with a: | |
|---|---|---|
| $_{YL}$ | | +14 |
| $_{r}$ | | +5 |
| $_{p}$ | **-126** | **+126** |
| $_{T}$ | **+152** | **-152** |
| $_{SGD}$ | **-45** | **+435** |
| $^{228}Ra_{YL}$ | | |
| $^{228}Ra_{r}$ | | |
| $^{228}Ra_{SGD}$ | **+249** | **-42** |
| | | |
| $_{r}$ | | +2 |
| $_{p}$ | **-57** | **+57** |
| $_{T}$ | **+69** | **-69** |
| $_{SGD}$ | **-45** | **+435** |
| $^{228}Ra_{r}$ | | |
| $^{228}Ra_{SGD}$ | **+249** | **-42** |